

# Dehydration behavior of FGD gypsum by simultaneous TG and DSC analysis

Wenbin Lou · Baohong Guan · Zhongbiao Wu

Received: 13 July 2010/Accepted: 6 October 2010/Published online: 26 October 2010  
© Akadémiai Kiadó, Budapest, Hungary 2010

**Abstract** The dehydration behaviors of FGD gypsums from three power plants were investigated at N<sub>2</sub> atmosphere (autogenous and negligible partial pressure of water,  $P_{\text{H}_2\text{O}}$ ) in non-isothermal and isothermal condition. The dehydration of gypsum proceeded through one step, i.e., CaSO<sub>4</sub>·2H<sub>2</sub>O →  $\gamma$ -CaSO<sub>4</sub> ( $\gamma$ -anhydrite) or two steps, i.e., CaSO<sub>4</sub>·2H<sub>2</sub>O → CaSO<sub>4</sub>·0.5H<sub>2</sub>O (hemihydrate) →  $\gamma$ -CaSO<sub>4</sub> depending on temperature and  $P_{\text{H}_2\text{O}}$ . The discrepancies of three FGD gypsums on dehydration behavior were very likely due to the different crystalline characteristics (size and habit) and impurities, such as fly ash and limestone. Experimental data of non-isothermal analysis have been fitted with two ‘model-free’ kinetic methods and those of isothermal analysis have been fitted with Avrami and linear equation. The apparent empirical activation energies ( $E_a$ ) suggest that the transition from gypsum to hemihydrate is mainly controlled by nucleation and growth mechanism, while the transition from gypsum to  $\gamma$ -anhydrite is mostly followed by phase boundary mechanism.

**Keywords** FGD gypsum · Dehydration behavior · Kinetics · TG/DSC · Crystalline characteristics

## Introduction

Calcium sulfate dihydrate (gypsum) is a commonly found mineral in the nature, and it is an important building

material in the production of ‘Plaster of Paris’, gypsum wallboard, and Portland cement [1, 2]. The CaSO<sub>4</sub>–H<sub>2</sub>O system is characterized at least five crystalline phases, which are gypsum (CaSO<sub>4</sub>·2H<sub>2</sub>O), hemihydrates ( $\alpha$ - and  $\beta$ -CaSO<sub>4</sub>·0.5H<sub>2</sub>O), soluble anhydrite ( $\gamma$ -CaSO<sub>4</sub>) and insoluble anhydrite (AIII-CaSO<sub>4</sub> and AII-CaSO<sub>4</sub>) [3].

A detailed knowledge of the conditions, mechanisms, and kinetics of the phase transitions in the CaSO<sub>4</sub>–H<sub>2</sub>O system is crucial for applications of CaSO<sub>4</sub>-based materials [1, 4]. For example, efforts have been made to obtain a product with a minimum amount of insoluble anhydrite during the production of Plaster of Paris [3]. The thermal dehydration processes have been extensively investigated as a function of temperature and partial pressure of water ( $P_{\text{H}_2\text{O}}$ ) with several experimental techniques. However, it is still obscure about the dehydration mechanism throughout the whole thermal process from gypsum to anhydrite and it is also uncertain about the routes of phase transitions during the dehydration process [5].

Most literature reported that gypsum dehydration undergoes a two-step process, CaSO<sub>4</sub>·2H<sub>2</sub>O → CaSO<sub>4</sub>·0.5H<sub>2</sub>O →  $\gamma$ -CaSO<sub>4</sub> [5–13], while some reports showed that  $\gamma$ -CaSO<sub>4</sub> is directly produced during gypsum dehydration [14–19] and hemihydrate is formed by rehydration of  $\gamma$ -CaSO<sub>4</sub> upon cooling with humid air [18, 19]. In fact, the two-step process was obtained at a certain  $P_{\text{H}_2\text{O}}$ , while the one-step process was achieved at negligible  $P_{\text{H}_2\text{O}}$ . Ball and Norwood [20] pointed out that both temperature and  $P_{\text{H}_2\text{O}}$  controlled the product of dehydration. The hemihydrate was produced only when the decomposition occurred at high  $P_{\text{H}_2\text{O}}$  and below 115 °C, while the anhydrite was formed above 115 °C and at low  $P_{\text{H}_2\text{O}}$ . Badens et al. [21] also reported that the final dehydration products were a function of  $P_{\text{H}_2\text{O}}$ . A two-step process happened at  $P_{\text{H}_2\text{O}}$  of 900 Pa,

W. Lou · B. Guan (✉) · Z. Wu  
Department of Environmental Engineering, Zhejiang University,  
Hangzhou 310027, China  
e-mail: guanbaohong@zju.edu.cn

W. Lou  
Department of Chemical Engineering, Ningbo University of  
Technology, Ningbo 315016, China

but no intermediate phase (hemihydrate) occurred at a  $P_{\text{H}_2\text{O}}$  of 1 and 500 Pa. However, one-step [18] and two-step [10] processes at negligible  $P_{\text{H}_2\text{O}}$  ( $\text{N}_2$  atmosphere) were separately reported by in situ IR investigation, which shows a contradiction.

From the viewpoint of potential rate-controlling steps in solid-state decomposition reactions, a lot of gypsum dehydration mechanisms have been proposed, such as ‘diminishing sphere’ or ‘diminishing plate’ [15], topotactic reaction [9], nucleation and growth [14, 20], phase boundary (i.e., that the rate-controlling step in the process is the migration of the hemihydrate–gypsum interface) [5, 12, 20], autocatalytic nucleation [5, 11, 22], and diffusion kinetic mechanism [20]. The dehydration kinetics varied with the temperature and  $P_{\text{H}_2\text{O}}$ . It was reported that the dehydration involved nucleating and boundary controlling between 353 and 383 K, but was controlled by a diffusion mechanism for 383–425 K [20]. Dos Santos et al. [12] reported that the dehydration was dominated by first-order kinetics above 383 K and a two-dimensional phase boundary mechanism below 373 K. It was also reported that the dehydration kinetics was a function of the degree of dehydration [11, 22, 23]. Expect for macroscopic investigation, an in situ study of dehydration process has been done using hydrothermal atomic force microscopy (HAFM) [24]. In that research, the lateral pit growth yielded an  $E_a$  of  $119 \pm 11 \text{ kJ mol}^{-1}$  (360–393 K), a value attributing to a phase boundary mechanism.

The dehydration behavior may vary significantly among different gypsum types, such as natural gypsum and many kinds of chemical gypsums [6, 23, 25, 26]. Differences in crystalline characteristics (i.e., size, habit, amount of defects) and impurities appear to be the most important factors resulting in discrepancies of dehydration behavior [4, 27]. Flue gas desulfurization (FGD) gypsum, one of the most important chemical gypsums, has been widely used in plaster-based construction material [28, 29] and the research on its dehydration behavior is of both scientific and practical interests. However, only little work has focused on the FGD gypsum dehydration behavior until now [26]. The origin, i.e., different plants, process route, and operating conditions brings to differences in crystalline characteristics [28], and thus affects the dehydration behavior.

This work is to investigate the dehydration behavior of FGD gypsum at both autogenous and negligible  $P_{\text{H}_2\text{O}}$  by simultaneous thermalgravimetry (TG) and differential scanning calorimetry (DSC) in both non-isothermal and (quasi-) isothermal conditions. Crystalline characteristics (size and habit) of FGD gypsum samples were analyzed at first to discuss the dehydration behavior discrepancies among them.

## Experimental

### Materials

FGD gypsums from three local power plants of Ban Shan (G1), Lan Xi (G2) and Qian Qin (G3) in Zhejiang Province, China, were adopted as raw material. The FGD gypsums were dried at 45 °C to a constant mass and passed 60-mesh sieve before all analyses. The chemical compositions of three FGD gypsums are presented in Table 1. The mass percentages of calcium sulfate dihydrate calculated by the content of  $\text{SO}_3$  are up to 94.3, 95.8, and 94.1%, respectively. The main impurities are some  $\text{SiO}_2$ , which could come from as amorphous phase of fly ash and crystal phase of quartz, the impurity of limestone. The  $\text{CO}_2$  comes from unreacted limestone.

### Methods

The dehydration process of FGD gypsum was performed with simultaneous TG/DSC analysis (NETZSCH STA 409 Luxx, Selb/Bavaria, Germany) at  $\text{N}_2$  atmosphere with a gas flow of 20 mL min<sup>-1</sup>. Non-isothermal analysis was carried out at different heating rate (2–20 K min<sup>-1</sup>). Isothermal analysis was conducted in the temperature range of 70–105 °C with a span of 5 °C and a heating rate of 1 K min<sup>-1</sup> was applied before the temperature reached the set one. Both thermal analyses used 70  $\mu\text{L}$  alumina crucible and sample mass was between 5.00 and 10.00 mg. An autogenous  $P_{\text{H}_2\text{O}}$  atmosphere was got when the crucible was covered with a pinhole lid, while a negligible one was achieved with no lid used. Data collected at two different atmospheres were used to distinguish the influence of  $P_{\text{H}_2\text{O}}$  on the dehydration of gypsum.

**Table 1** Chemical compositions of three FGD gypsums

Oxides/elements	Chemical compositions (wt%)		
	G1	G2	G3
CaO	31.76	32.26	31.84
$\text{SO}_3$	43.87	44.56	43.79
$\text{SiO}_2$	2.00	0.87	1.85
$\text{CO}_2$	0.82	0.94	0.32
$\text{Al}_2\text{O}_3$	0.25	0.08	0.24
$\text{Fe}_2\text{O}_3$	0.10	0.05	0.12
MgO	0.03	0.05	0.05
$\text{K}_2\text{O}$	0.03	0.02	0.06
$\text{Na}_2\text{O}$	<0.01	0.02	0.05
IL (300 °C)	19.88	20.10	20.22
Total	98.72	98.95	98.54

The particle size distribution (PSD) of FGD gypsum was tested by a laser particle size analyzer (Mastersizer 2000, Malvern, England) after being dispersed in anhydrous ethanol with an ultrasonic bath. The crystal habit was observed by a Scanning Electron Microscope (SEM, SIRION-100, FEI Company, USA). The samples were examined with X-ray diffraction (XRD, D/Max-2550 pc, Rigaku Inc., Japan) using Cu  $\kappa\alpha$  radiation at a scanning rate of 8°/min.

## Results and discussion

### Crystal characteristics analysis

The PSDs of three FGD gypsums are shown in Fig. 1. The grains are mainly distributed between 10 and 150  $\mu\text{m}$ . The volume weighted mean diameters of G1, G2, and G3 are 52.2, 42.6 and 33.9  $\mu\text{m}$ , respectively, which agrees with the particle diameters range (35–70  $\mu\text{m}$ ) of another FGD gypsum sample reported by Cave and Holdich [26]. However, the natural gypsum is always out of this range.

Figure 2 shows the morphologies of three FGD gypsums by SEM. G1 and G2 show regular rhombic crystals, which implies the crystals are well developed, while G3 shows irregular appearance, which means the crystals are not well grown. A lot of micro-spheres of fly ash cover the surfaces of gypsum crystals. The differences of size and habit among the three FGD gypsums are mainly caused by the operation parameters in desulphurization unit. Crystal residence time has an essential influence on the growth of gypsum crystals, a short residence time produces small and irregular gypsum crystals and vice versa [28].

The X-ray diffraction patterns of three FGD gypsums are shown in Fig. 3. G1 and G2 have similar relative reflection intensities on different crystal surfaces, but they are quite different with G3. The intensities on the (−121),

(002), and (022) surfaces of G3 are stronger than that of G1 and G2, while the intensity on the (020) surface of G3 is much weaker. Morphological images and XRD patterns of the FGD gypsums suggest a correction of the X-ray absorption through the occurrence of crystal forms, although it is not always the case [30]. A number of studies indicate that gypsum crystals are to be classified as mosaic crystals, whereby size, amount and disorder of orientation of the blocks are largely dependent on the conditions presented during crystallization [30]. Hence, the PSDs, morphologies and XRD patterns of the three FGD gypsums reveal the difference of conditions under which the FGD gypsums were produced.

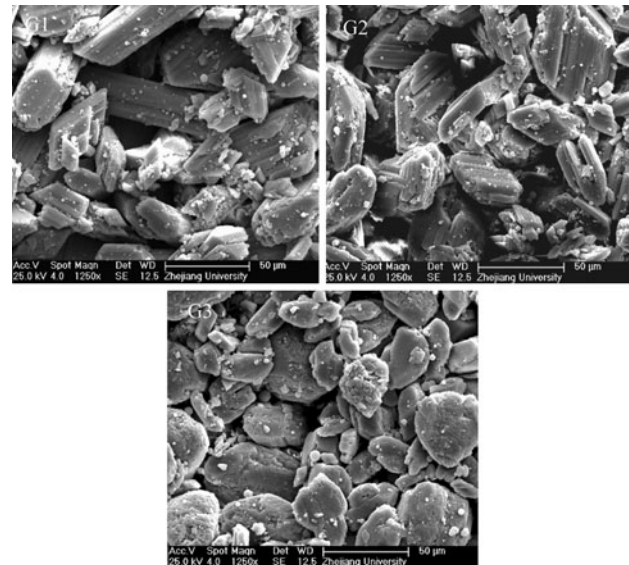


**Fig. 2** SEM images of three FGD gypsums

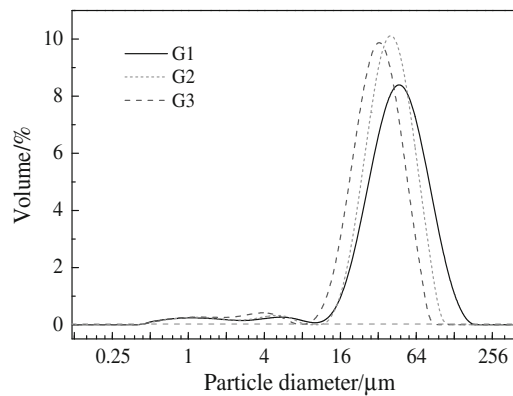


**Fig. 1** Particle size distributions of three FGD gypsums

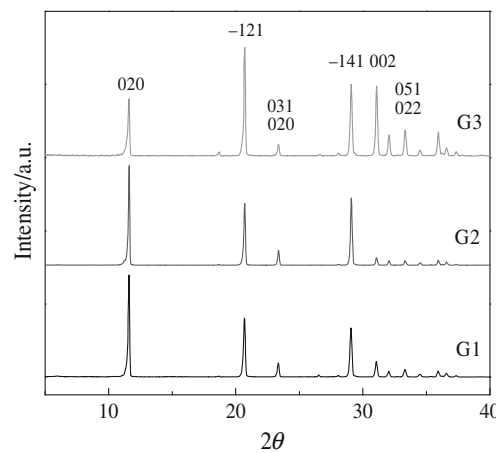


**Fig. 3** XRD patterns of three FGD gypsums

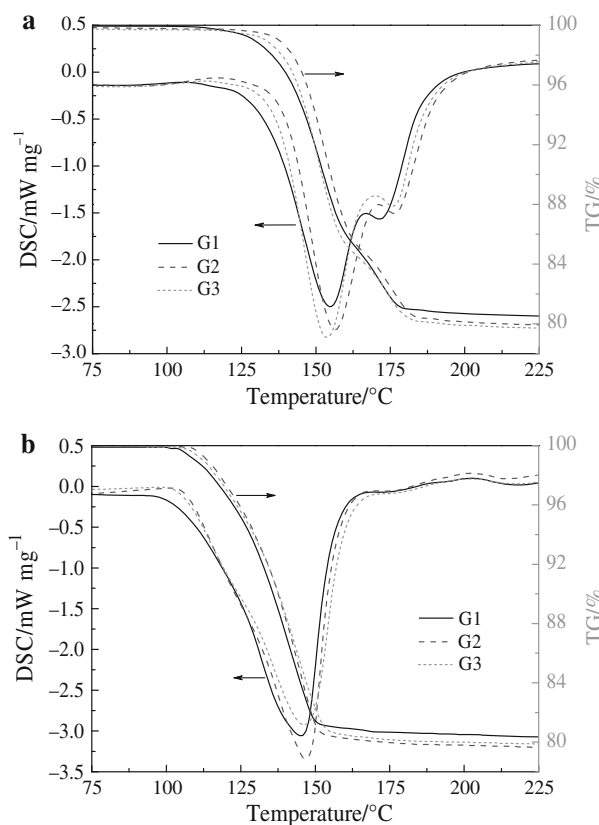


**Fig. 4** TG and DSC curves of three FGD gypsums dehydration at heating rates of  $10 \text{ K min}^{-1}$ : **a** at autogenous  $P_{\text{H}_2\text{O}}$  atmosphere and **b** at negligible  $P_{\text{H}_2\text{O}}$  atmosphere

#### Non-isothermal dehydration analysis

Figure 4 shows the TG and DSC curves of three FGD gypsums dehydration at heating rate of  $10 \text{ K min}^{-1}$ . At autogenous  $P_{\text{H}_2\text{O}}$  atmosphere (Fig. 4a), the gypsums break down thermally in two processes apparently. This is the case that a lot of researchers believe that gypsum dehydration undergoes a two-step process of  $\text{CaSO}_4 \cdot 2\text{H}_2\text{O} \rightarrow \text{CaSO}_4 \cdot 0.5\text{H}_2\text{O} \rightarrow \gamma\text{-CaSO}_4$ . The two ‘jumps’ of a 3:1 mass loss in TG curves are consistent with the stoichiometry of the dehydration reactions, which confirms the two-step dehydration process. However, the real dehydration route may be covered by the data of macro-mass loss. The two DSC peaks are partly overlapped, indicating that hemihydrate begins to transit to anhydrite before dihydrate completes its transformation to hemihydrate. Therefore, three phases of calcium sulfate coexist during certain dehydration period. Because the existence of hemihydrate strongly depends on  $P_{\text{H}_2\text{O}}$  and temperature [20, 21], the ideal two-step dehydration process could not be achieved in the experimental condition of this work.

At negligible  $P_{\text{H}_2\text{O}}$  atmosphere (Fig. 4b), the successive mass loss and the only one endothermal peak make gypsum seem to dehydrate via one step, i.e.,  $\text{CaSO}_4 \cdot 2\text{H}_2\text{O} \rightarrow \gamma\text{-CaSO}_4$ . However, it may not be the real way. If the hemihydrate formed as intermediate, loses its 0.5 crystal  $\text{H}_2\text{O}$  very quickly, the same TG and DSC curves could also be achieved. In fact, the similarity of  $\gamma$ -anhydrite and hemihydrate in crystal structure has proven that hemihydrate and  $\gamma$ -anhydrite can transform to each other very quickly [14]. So, the TG/DSC analysis data got here can not give a definite answer about the real dehydration route of gypsum because the thermal analysis is a macroscopic technique and cannot determine the process at a local level. It is the reason that a lot of analyses with in situ phase detection were carried out to find out the real gypsum dehydration process as mentioned in introduction [5, 10, 14, 18, 24]. However, debates have not ended until now.

It shows that gypsum dehydrates more easily at negligible  $P_{\text{H}_2\text{O}}$  atmosphere. As the principle of reaction equilibrium, the produced water increases the  $P_{\text{H}_2\text{O}}$  in the crucible with a pinhole lid, and thus higher temperature is needed to promote the dehydration. As a result, an ‘induction period’ appears in the gypsum dehydration at autogenous  $P_{\text{H}_2\text{O}}$ , while no such ‘induction period’ exists at negligible  $P_{\text{H}_2\text{O}}$ . It is also found out that the dehydration endset temperatures at autogenous  $P_{\text{H}_2\text{O}}$  (around  $180^\circ\text{C}$ ) are much higher than those at negligible  $P_{\text{H}_2\text{O}}$  (around  $150^\circ\text{C}$ ).

The differences in TG and DSC profiles among the three gypsums indicate the influence of sample origin on dehydration behavior. The most obvious discrepancy is the temperature, at which gypsum begins to dehydrate. G1 begins to dehydrate at lowest temperature, while G2 begins to dehydrate at highest temperature at both  $P_{\text{H}_2\text{O}}$  atmospheres (Fig. 4). The covered fly ash (Fig. 2), the main impurity, may bring on such difference, because the impurities may accelerate the dehydration of gypsum [27]. In the main range of gypsum dehydration, the TG and DSC profiles of G2 and G3 are parallel with each other. However, G1 has a little slower mass loss rate than those of G2 and G3 and it may attribute to its coarser particles (Fig. 1). G2 and G3 show quite similar dehydration behavior despite the discrepancies of crystalline characteristics. For this reason, G1 and G2 were chosen to investigate their dehydration kinetics.

#### Isothermal dehydration analysis

Figure 5 shows the TG and DSC curves of G1 in isothermal condition (autogenous  $P_{\text{H}_2\text{O}}$  atmosphere). The oscillations of temperature and DSC are due to the regulation system which switches on and off heating for adjusting

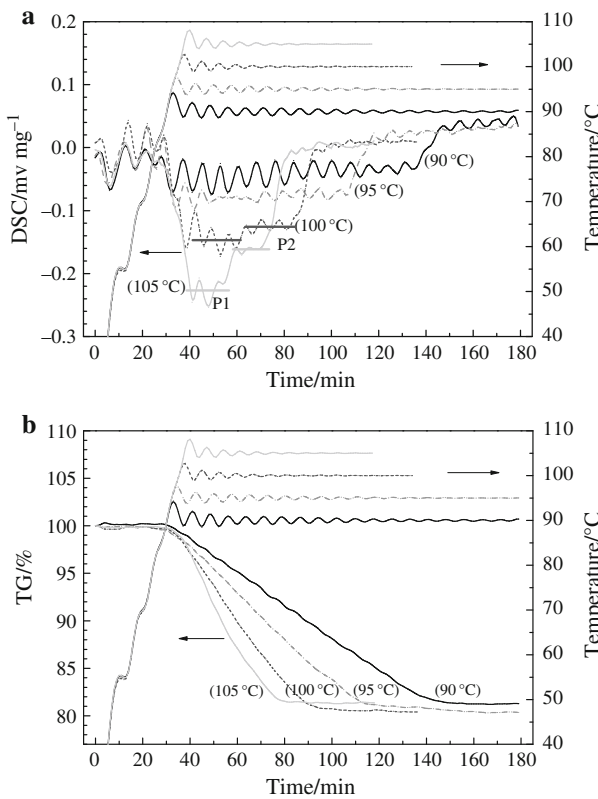


**Fig. 5** DSC (a) and TG (b) curves of G1 dehydration in isothermal condition at autogenous  $P_{H_2O}$

temperature to the programmed one. The regular fluctuation of DSC profile and the linear decline of TG at 90 and 95 °C imply that the dehydration proceeds as one step, i.e.,  $\text{CaSO}_4 \cdot 2\text{H}_2\text{O} \rightarrow \gamma\text{-CaSO}_4$ . The same behavior has also been observed at lower temperature.

However, at 100 and 105 °C, the DSC profiles show two platforms (marked with thick line, P1 and P2), which implies that the dehydration process is modified. This phenomenon attributes to the elevated  $P_{H_2O}$  at higher temperatures. Gypsum dehydrates more quickly and the autogenous  $P_{H_2O}$  increases when temperature rises, and then the one-step dehydration process is modified by the two-step dehydration process, where hemihydrate is the metastable phase.

At negligible  $P_{H_2O}$  atmosphere (70–95 °C), G1 undergoes one-step dehydration process without modified phenomenon and the result would not be present here.

#### Kinetics of FGD gypsum dehydration

A mathematical description of chemical reaction data is usually sought in terms of a ‘kinetic triplet’ (i.e., Arrhenius parameters  $A$  and  $E_a$ , and the reaction model,  $f(\alpha)$ , also

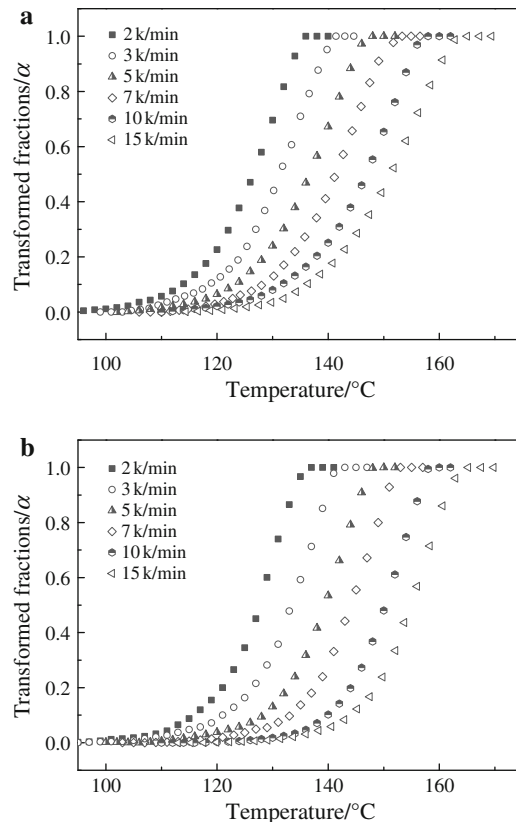


**Fig. 6** Transformed fraction ( $\alpha$ ) versus temperature curves for the dehydration (gypsum to hemihydrate) of G1 (a) and G2 (b), heating rates: 2, 3, 5, 7, 10 and 15 K min<sup>-1</sup>

called the conversion function), which is related to the experimental data as follows [31, 32]:

$$\frac{d\alpha}{dt} = A \exp(-E_a/RT) f(\alpha). \quad (1)$$

For non-isothermal data obtained at a constant heating rate  $\beta = dT/dt$ ,  $d\alpha/dt$  in Eq. 1 is replaced with  $\beta d\alpha/dT$ .

#### Non-isothermal analysis

Experimental data got from non-isothermal analysis of G1 and G2 at different heating rates (2, 3, 5, 7, 10 and 15 K min<sup>-1</sup>) at autogenous  $P_{H_2O}$  are shown in Fig. 6. The transformed fraction ( $\alpha$ ) were calculated as the first mass ‘jump’ (Fig. 4a), which corresponds to the transition from gypsum to hemihydrate, although it is not an ideal process of  $\text{CaSO}_4 \cdot 2\text{H}_2\text{O} \rightarrow \text{CaSO}_4 \cdot 0.5\text{H}_2\text{O}$  as mentioned above.

Experimental data got from non-isothermal analysis of G1 and G2 at different heating rates (3, 5, 7, 10, 15 and 20 K min<sup>-1</sup>) at negligible  $P_{H_2O}$  are shown in Fig. 7. The transformed fractions ( $\alpha$ ) were calculated as the whole mass loss (Fig. 4b), which corresponds to the transition from gypsum to  $\gamma$ -anhydrite.

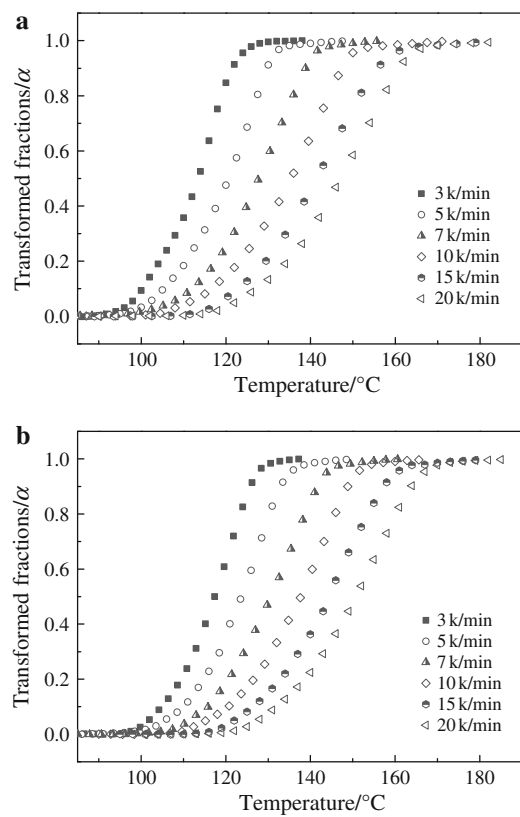


**Fig. 7** Transformed fraction ( $\alpha$ ) versus temperature curves for the dehydration (gypsum to  $\gamma$ -anhydrite) of G1 (a) and G2 (b), heating rates: 3, 5, 7, 10, 15, and  $20\text{ K min}^{-1}$

A lot of kinetic methods are ready to describe mathematically the data, involving at least one kinetic triplet of parameters [31]. Because of the inconsistency of gypsum dehydration kinetics models reported, two ‘model-free’ kinetic methods were employed to calculate the activation energy ( $E_a$ ) in non-isothermal analysis. The first one is the iso-conversional method of Flynn, Wall and Ozawa as shown as [31]

$$\ln(\beta) = \ln[Af(\alpha)/(d\alpha/dT)] - E_a/RT, \quad (2)$$

which involves measuring the temperatures corresponding to the fixed values of  $\alpha$  at different heating rates,  $\beta$ , and plotting  $\ln(\alpha)$  against  $1/T$ . The slopes of such plots give  $-E_a/R$ .

The second one is the ‘general method’ as shown as [31]

$$\ln(d\alpha/dT) = \ln(Af(\alpha)/\beta) - E_a/RT. \quad (3)$$

From a number of ( $\alpha$ ,  $T$ ) values from one non-isothermal experiment, the left side of equation may be calculated and plotted versus  $1/T$ . The slopes of such plots also give  $-E_a/R$ .

The calculated  $E_a$  values at autogenous  $P_{\text{H}_2\text{O}}$  ( $\text{CaSO}_4 \cdot 2\text{H}_2\text{O} \rightarrow \text{CaSO}_4 \cdot 0.5\text{H}_2\text{O}$ ) and at negligible  $P_{\text{H}_2\text{O}}$  ( $\text{CaSO}_4 \cdot 2\text{H}_2\text{O} \rightarrow \gamma\text{-CaSO}_4$ ) are presented in Tables 2 and 3, respectively. The discrepancy of  $E_a$  values by ‘Flynn, Wall and Ozawa’ and ‘general’ method indicates the influence of kinetic methods chosen. The  $E_a$  values of G1 at both autogenous and negligible  $P_{\text{H}_2\text{O}}$  are smaller than that of G2, which may attribute to their crystalline characteristics and impurities.

At autogenous  $P_{\text{H}_2\text{O}}$ , the  $E_a$  values of  $161 \pm 8\text{ kJ mol}^{-1}$  (G1) and  $194 \pm 18\text{ kJ mol}^{-1}$  (G2) at low  $\alpha$  by Flynn, Wall, Ozawa method (Table 2) are reasonably in the range ( $145\text{--}247\text{ kJ mol}^{-1}$ ) attributed to a nucleation and growth reaction kinetics [20], while at high  $\alpha$ , the  $E_a$  values of  $111 \pm 12\text{ kJ mol}^{-1}$  (G1) and  $136 \pm 11\text{ kJ mol}^{-1}$  (G2) are slightly smaller than that.

The  $E_a$  values of  $154\text{ kJ mol}^{-1}$  (G1) and  $169\text{ kJ mol}^{-1}$  (G2) at low heating rate and  $157\text{ kJ mol}^{-1}$  (G1) and  $173\text{ kJ mol}^{-1}$  (G2) at high heating rate by ‘General’ method are also reasonably in the  $E_a$  range following nucleation and growth reaction kinetics. During the fitting, it was found that the data were dispersive at both low and high  $\alpha$ . So the present  $E_a$  values here are the fitting results of medial  $\alpha$  (0.2–0.6).

At negligible  $P_{\text{H}_2\text{O}}$ , the  $E_a$  values of  $78 \pm 6\text{ kJ mol}^{-1}$  (G1) and  $79 \pm 7\text{ kJ mol}^{-1}$  (G2) at higher  $\alpha$  by Flynn, Wall, Ozawa method (Table 3) are slightly smaller than the values ( $80\text{--}97\text{ kJ mol}^{-1}$ ) attributed to a boundary control [20]. Whereas, the  $E_a$  values of  $130 \pm 11\text{ kJ mol}^{-1}$  (G1) and  $136 \pm 13\text{ kJ mol}^{-1}$  (G2) at lower  $\alpha$  are close to the values attributed to a nucleation and growth reaction kinetics. In both autogenous and negligible  $P_{\text{H}_2\text{O}}$ , the different  $E_a$  values of low and high  $\alpha$  obtained from method of Flynn, Wall and Ozawa suggest dehydration kinetics is a function of the degree of dehydration [11, 22, 23].

**Table 2** Kinetics methods and  $E_a$  values calculated for the non-isothermal analysis at autogenous  $P_{\text{H}_2\text{O}}(\text{CaSO}_4 \cdot 2\text{H}_2\text{O} \rightarrow \text{CaSO}_4 \cdot 0.5\text{H}_2\text{O})$

FGD gypsum	Method	$E_a/\text{kJ mol}^{-1}$
G1	Flynn, Wall, Ozawa	
	Low $\alpha$ (0.1–0.4)	$161 \pm 8$
G1	High $\alpha$ (0.5–0.9)	$111 \pm 12$
	General	
G2	Low heating rate, $\beta = 2$	154
	High heating rate, $\beta = 15$	157
G2	Flynn, Wall, Ozawa	
	Low $\alpha$ (0.1–0.4)	$194 \pm 18$
G2	High $\alpha$ (0.5–0.9)	$136 \pm 11$
	General	
	Low heating rate, $\beta = 2$	169
	High heating rate, $\beta = 15$	173

**Table 3** Kinetics methods and  $E_a$  values calculated for the non-isothermal analysis at negligible  $P_{H_2O}$ ( $\text{CaSO}_4 \cdot 2\text{H}_2\text{O} \rightarrow \gamma - \text{CaSO}_4$ )

FGD gypsum	Method	$E_a/\text{kJ mol}^{-1}$
G1	Flynn, Wall, Ozawa	
	Low $\alpha$ (0.1–0.4)	130 ± 11
	High $\alpha$ (0.5–0.9)	78 ± 6
G1	General	
	Low heating rate, $\beta = 3$	82
	High heating rate, $\beta = 20$	72
G2	Flynn, Wall, Ozawa	
	Low $\alpha$ (0.1–0.4)	136 ± 13
	High $\alpha$ (0.5–0.9)	79 ± 7
G2	General	
	Low heating rate, $\beta = 3$	98
	High heating rate, $\beta = 20$	75

The calculated  $E_a$  values ('General' method) of 82  $\text{kJ mol}^{-1}$  (G1) and 98  $\text{kJ mol}^{-1}$  (G2) at low heating rate are reasonably in the range (80–97  $\text{kJ mol}^{-1}$ ) attributed to a boundary control, while the values of 72  $\text{kJ mol}^{-1}$  (G1) and 75  $\text{kJ mol}^{-1}$  (G2) at high heating rate are slightly smaller than that [20]. The close  $E_a$  values at low and high heating rates indicate the 'General' method is not sensitive with the selected heating rate.

It is speculated that the transition of gypsum to hemihydrate follows nucleation and growth reaction kinetics, while the transition of gypsum to  $\gamma$ -anhydrite is controlled by a phase boundary mechanism in this research condition. The  $E_a$  values in non-isothermal analysis are no kinetics model included and thus the dehydration kinetics are just speculated from  $E_a$  values. So model involved method would be applied to investigate the dehydration kinetics in isothermal analysis.

#### Isothermal analysis

Experimental data got from isothermal analysis of G1 at both autogenous  $P_{H_2O}$  (75–95 °C) and negligible  $P_{H_2O}$  (70–95 °C) are shown in Fig. 8. The transformed fractions ( $\alpha$ ) were calculated as the whole mass loss, which corresponds to the transition from gypsum to anhydrite. Experimental data have been tentatively fitted with models with acceleratory  $\alpha$ -time curves and deceleratory  $\alpha$ -time curves based on geometrical, diffusion and order of reaction mechanism [27]. But poor fittings imply that those mechanisms are not adequate to describe the process. Then data were fitted with Avrami equation, model with sigmoidal  $\alpha$ -time curves, under general form as [5, 31]

$$\alpha = 1 - \exp^{(-kt)^n}, \quad (4)$$

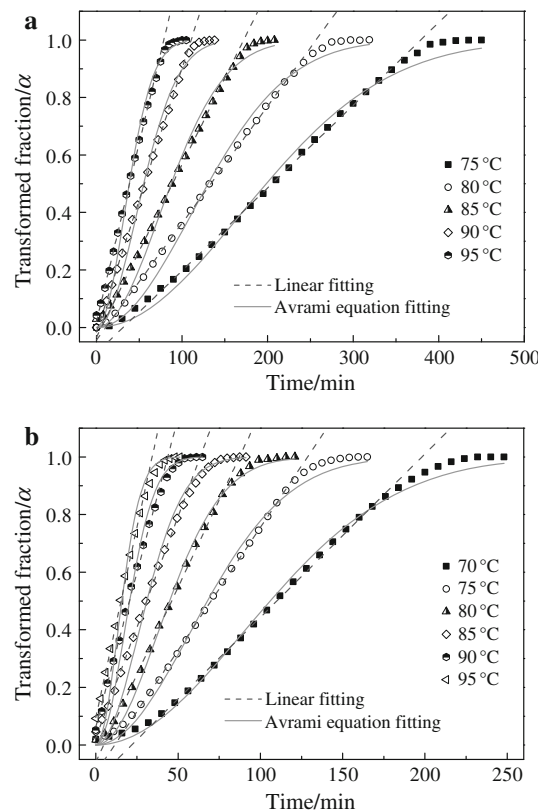


**Fig. 8** Transformed fraction ( $\alpha$ ) versus time curves for the dehydration (gypsum to  $\gamma$ -anhydrite) of G1, **a** at autogenous  $P_{H_2O}$ , temperature range 75–95 °C; **b** at negligible  $P_{H_2O}$ , temperature range 70–95 °C

**Table 4** Rate constants  $k$  and corresponding correlation values  $R^2$  obtained by fitting of transformed fraction versus time data with the Avrami equation and linear fitting, at autogenous  $P_{H_2O}$ , G1

Temperature/°C	Avrami equation fitting		Linear fitting	
	$R^2$	$k$	$R^2$	$k$
75	0.9937	$4.20 \times 10^{-3}$	0.9989	$2.88 \times 10^{-3}$
80	0.9913	$6.38 \times 10^{-3}$	0.9992	$4.07 \times 10^{-3}$
85	0.9881	$9.55 \times 10^{-3}$	0.9995	$6.01 \times 10^{-3}$
90	0.9862	$1.51 \times 10^{-2}$	0.9998	$9.18 \times 10^{-3}$
95	0.9795	$2.17 \times 10^{-2}$	0.9985	$1.24 \times 10^{-2}$

where  $k$  is the rate constant, and  $n$  is the parameter describing the dimension of the reaction mechanism.

In the first fitting run, the  $n$  distributed between 2 (70 °C) and 1.5 (95 °C). So in the second fitting run, the  $n$  was fixed to 2. For the linear profiles of data (except for low and high  $\alpha$ ), linear fitting was also employed with  $\alpha$  values from 0.1 to 0.9. The fitting curves are presented in Fig. 8 and the rate constant  $k$  and the corresponding correlation value  $R^2$  for each temperature are shown in

Table 4 (at autogenous  $P_{\text{H}_2\text{O}}$ ) and Table 5 (at negligible  $P_{\text{H}_2\text{O}}$ ), respectively.

Rate constants  $k$  obtained from the various temperatures were plotted against temperature as  $\ln k$  versus  $1/T$ , i.e., the logarithmic form of the Arrhenius equation:

$$\ln k = \ln A - E_a/RT. \quad (5)$$

Under this form, the slope of plot provides the  $E_a$  (Fig. 9).

The  $\ln k$  is linearly dependent on  $1/T$  (Fig. 9), which clearly indicates that the dehydration follows a single mechanism within the experimental temperature range.

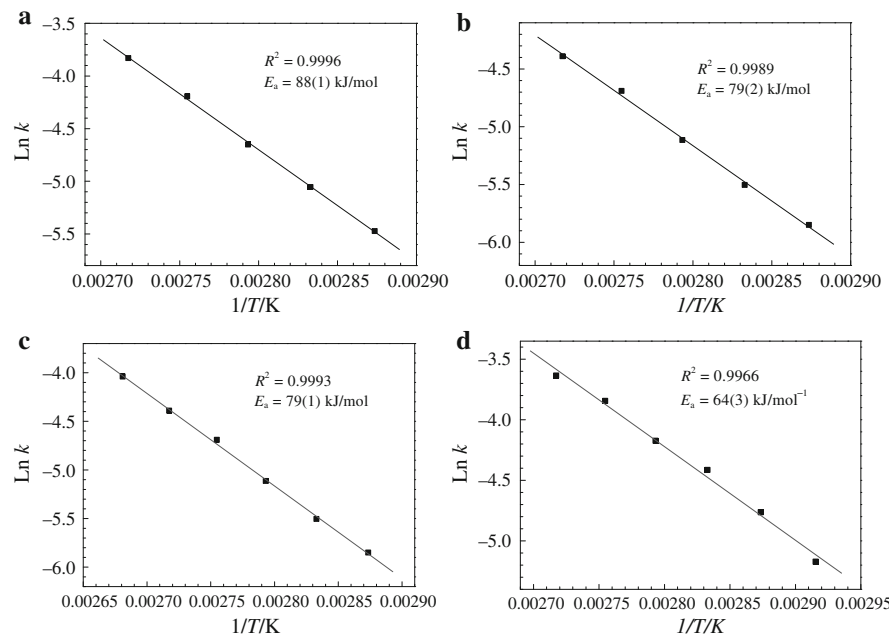
**Table 5** Rate constants  $k$  and corresponding correlation values  $R^2$  obtained by fitting of transformed fraction vs time data with the Avrami equation and linear fitting, at negligible  $P_{\text{H}_2\text{O}}$ , G1

Temperature (°C)	Avrami equation fitting		Linear fitting	
	$R^2$	$k$	$R^2$	$k$
70	0.9962	$7.86 \times 10^{-3}$	0.9985	$5.67 \times 10^{-3}$
75	0.9945	$1.23 \times 10^{-2}$	0.9995	$8.53 \times 10^{-2}$
80	0.9954	$1.86 \times 10^{-2}$	0.9968	$1.21 \times 10^{-2}$
85	0.9788	$2.69 \times 10^{-2}$	0.9975	$1.54 \times 10^{-2}$
90	0.9673	$4.04 \times 10^{-2}$	0.9953	$2.14 \times 10^{-2}$
95	0.9449	$5.27 \times 10^{-2}$	0.9981	$2.64 \times 10^{-2}$

The result agrees with some other reports [5, 10]. The  $E_a$  values at autogenous  $P_{\text{H}_2\text{O}}$  ( $88 \pm 1 \text{ kJ mol}^{-1}$  with Avrami equation fitting and  $79 \pm 2 \text{ kJ mol}^{-1}$  with linear fitting) are both reasonably close to the range ( $80\text{--}97 \text{ kJ mol}^{-1}$ ) attributed to a boundary control [20]. The  $E_a$  values at negligible  $P_{\text{H}_2\text{O}}$  ( $79 \pm 1 \text{ kJ mol}^{-1}$  with Avrami equation fitting and  $64 \pm 3 \text{ kJ mol}^{-1}$  with linear fitting) are slightly smaller than that. It is reasonable that the  $E_a$  values at autogenous  $P_{\text{H}_2\text{O}}$  are slightly bigger than those at negligible  $P_{\text{H}_2\text{O}}$  for the elevated  $P_{\text{H}_2\text{O}}$  [6].

The  $E_a$  values in isothermal analysis are quite close to  $75 \pm 8 \text{ kJ mol}^{-1}$  [14] and  $81 \text{ kJ mol}^{-1}$  (FGD gypsum sample) [26], which were both fitted with the two-dimensional Avrami expression. However, the  $E_a$  values are in general smaller than those reported in the range of  $90\text{--}96 \text{ kJ mol}^{-1}$  [10, 16, 20],  $100.5 \pm 1.2 \text{ kJ mol}^{-1}$  ( $\alpha = 0.1\text{--}0.7$ ) [11],  $109 \pm 12 \text{ kJ mol}^{-1}$  [5],  $108\text{--}116 \text{ kJ mol}^{-1}$  [6] and  $119 \pm 11 \text{ kJ mol}^{-1}$  [24]. The differences for  $E_a$  values with those found in references are reasonably due to different experimental conditions, such as temperature range,  $P_{\text{H}_2\text{O}}$  and fluxing type [5]. The sample origin (FGD gypsum) may also play an important role in dehydration kinetics. The impurities such as fly ash may accelerate gypsum to dehydrate, and thereby decrease the  $E_a$  values.

**Fig. 9** Arrhenius  $\ln k$  versus  $1/T$  plot for gypsum (G1) to  $\gamma$ -anhydrite conversion at autogenous  $P_{\text{H}_2\text{O}}$  **a** Avrami equation fitting, **b** linear fitting, and at negligible  $P_{\text{H}_2\text{O}}$ , **c** Avrami equation fitting, **d** linear fitting



## Conclusions

The dehydration behavior of FGD gypsums depends on temperature and  $P_{\text{H}_2\text{O}}$ . One-step process (i.e.,  $\text{CaSO}_4 \cdot 2\text{H}_2\text{O} \rightarrow \gamma\text{-CaSO}_4$ ) occurs at negligible  $P_{\text{H}_2\text{O}}$  in non-isothermal condition and below 100 °C in isothermal condition, while two-step process (i.e.,  $\text{CaSO}_4 \cdot 2\text{H}_2\text{O} \rightarrow \text{CaSO}_4 \cdot 0.5\text{H}_2\text{O} \rightarrow \gamma\text{-CaSO}_4$ ) occurs at autogenous  $P_{\text{H}_2\text{O}}$  in non-isothermal condition and above 100 °C in isothermal condition (at autogenous  $P_{\text{H}_2\text{O}}$ ).

The  $E_a$  values suggest that the dehydration process of gypsum at low  $P_{\text{H}_2\text{O}}$  ( $\text{CaSO}_4 \cdot 2\text{H}_2\text{O} \rightarrow \gamma\text{-CaSO}_4$ ) is mainly dominated by boundary control mechanism, while it is mostly controlled by nucleation and growth mechanism at high  $P_{\text{H}_2\text{O}}$  ( $\text{CaSO}_4 \cdot 2\text{H}_2\text{O} \rightarrow \text{CaSO}_4 \cdot 0.5\text{H}_2\text{O}$ ).

The differences of the three FGD gypsums on crystalline characteristics (size and habit) and impurities such as fly ash and limestone likely result in the discrepancies of dehydration behavior among them.

**Acknowledgements** The authors acknowledge greatly the financial support of this work by the fund of Chinese National Program for High Technology Research and Development (Project No. 2006AA03Z385), Science and Technology Plan of Zhejiang Province, China (Project No. 2007C23055).

## References

1. Freyer D, Voigt W. Crystallization and phase stability of  $\text{CaSO}_4$  and  $\text{CaSO}_4$ -based salts. *Monatsh Chem.* 2003;134:693–719.
2. Solberg C, Evju C, Emanuelson A, Hansen S. Crystal structures of cementitious compounds. Part 3: calcium sulfates. *ZKG Int.* 2002;55:94–7.
3. Christensen AN, Olesen M, Cerenius Y, Jensen TR. Formation and transformation of five different phases in the  $\text{CaSO}_4 \cdot \text{H}_2\text{O}$  system: crystal structure of subhydrate  $\beta\text{-CaSO}_4 \cdot 0.5\text{H}_2\text{O}$  and soluble anhydrite  $\text{CaSO}_4$ . *Chem Mater.* 2008;20:2124–32.
4. Charola AE, Pühringer J, Steiger M. Gypsum: a review of its role in the deterioration of building materials. *Environ Geol.* 2007; 52:339–52.
5. Ballirano P, Melis E. Thermal behaviour and kinetics of dehydration of gypsum in air from in situ real-time laboratory parallel-beam X-ray powder diffraction. *Phys Chem Mineral* 2009;36: 391–402.
6. McAdie HG. The effect of water vapor upon the dehydration of  $\text{CaSO}_4 \cdot 2\text{H}_2\text{O}$ . *Can J Chem.* 1964;42:792–801.
7. Bushuev NN, Maslennikov BM, Borisov VM. X-ray diffraction investigation of  $\text{CaSO}_4 \cdot 0.67\text{H}_2\text{O}$ . *Russ J Inorg Chem.* 1982;27: 341–3.
8. Christensen AN, Lehmann MS, Pannetier J. A time-resolved neutron powder diffraction investigation of the hydration of  $\text{CaSO}_4 \cdot 1/2\text{D}_2\text{O}$  and of the dehydration of  $\text{CaSO}_4 \cdot 2\text{D}_2\text{O}$ . *J Appl Cryst.* 1985;18:170–2.
9. Abriel W, Reisdorf K, Pannetier J. Dehydration reactions of gypsum: a neutron and X-ray diffraction study. *J Solid State Chem.* 1990;85:23–30.
10. Putnis A, Winkler B. In situ IR spectroscopic and thermogravimetric study of the dehydration of gypsum. *Mineral Mag.* 1990;54:123–8.
11. Strydom CA, Hudson-Lamb DL, Potgieter JH, Dagg E. The thermal dehydration of synthetic gypsum. *Thermochim Acta.* 1995;269(270):631–8.
12. Dos Santos VA, Pereira JAFL, Dantas CC. Kinetics of thermal dehydration of gypsum ore for obtaining beta hemihydrate in a fluidized bed. *Bull Soc Chim Belg.* 1997;6:253–60.
13. Chang H, Huang PJ, Hou SC. Application of thermo-Raman spectroscopy to study dehydration of  $\text{CaSO}_4 \cdot 2\text{H}_2\text{O}$  and  $\text{CaSO}_4 \cdot 0.5\text{H}_2\text{O}$ . *Mater Chem Phys.* 1999;58:12–9.
14. Carbone M, Ballirano P, Caminiti R. Kinetics of gypsum dehydration at reduced pressure: an energy dispersive X-ray diffraction study. *Eur J Mineral.* 2008;20:621–7.
15. Molony B, Ridge MJ. Kinetics of the dehydration of calcium sulphate dihydrate in vacuo. *Aust J Chem.* 1968;21:1063–5.
16. Sarma LP, Prasad PSR, Ravikumar N. Raman spectroscopic study of phase transitions in natural gypsum. *J Raman Spectrosc.* 1998;29:851–6.
17. Prasad PSR, Pradhan A, Gowd TN. In situ micro-Raman investigation of dehydration mechanism in natural gypsum. *Curr Sci.* 2001;80:1203–7.
18. Chio CH, Sharma SK, Muenow DW. Micro-Raman studies of gypsum in the temperature range between 9 K and 373 K. *Am Mineral.* 2004;89:390–5.
19. Prasad PSR, Chaitanya VK, Prasad KS, Rao DN. Direct formation of the  $\gamma\text{-CaSO}_4$  phase in dehydration process of gypsum: in situ FTIR study. *Am Mineral.* 2005;90:672–8.
20. Ball MC, Norwood LS. Studies in the system calcium sulphate-water. Part I. Kinetics of dehydration of calcium sulphate dihydrate. *J Chem Soc A.* 1969;1633–7.
21. Badens E, Llewellyn P, Fulconis JM, Jourdan Veesler CS, Boistelle R, et al. Study of gypsum dehydration by controlled transformation rate thermal analysis (CRTA). *J Solid State Chem.* 1998;139:37–44.
22. Fatu D. Kinetics of gypsum dehydration. *J Therm Anal Calorim.* 2001;65:213–20.
23. Hudson-Lamb DL, Strydom CA, Potgieter JH. The thermal dehydration of natural gypsum and pure calcium sulphate dehydrate (gypsum). *Thermochim Acta.* 1996;282(283):483–92.
24. Jordan G, Astilleros JM. In situ HAFM study of the thermal dehydration on gypsum (010) surfaces. *Am Mineral.* 2006;91: 619–27.
25. Strydom CA, Potgieter JH. Dehydration behaviour of a natural gypsum and a phosphogypsum during milling. *Thermochim Acta.* 1999;332:89–96.
26. Cave SR, Holdich RG. The dehydration kinetics of gypsum in a fluidized bed reactor. *Chem Eng Res Des.* 2000;78:971–8.
27. Deutsch Y, Nathan Y, Sarig S. Thermogravimetric evaluation of the kinetics of the gypsum-hemihydrate-soluble anhydrite transitions. *J Therm Anal Calorim.* 1994;42:159–74.
28. Hamm H, Kersten HJ, Hueller R. 25 years experience gained in the European Gypsum Industry with the use of FGD gypsum. *CEM Int.* 2004;4:92–102.
29. Guan B, Yang L, Wu Z, Shen Z, Ma X, Ye Q. Preparation of  $\alpha$ -calcium sulfate hemihydrate from FGD gypsum in K, Mg-containing concentrated  $\text{CaCl}_2$  solution under mild conditions. *Fuel.* 2009;88:1286–93.
30. Follner S, Wolter A, Helming K, Silber C, Bartels H, Follner H. On the real structure of gypsum crystals. *Cryst Res Tech.* 2002;37:207–18.
31. Brown ME, Maciejewski M, Vyazovkin S, Nomen R, Sempere J, Burnham A, et al. Computational aspects of kinetic analysis. Part A: the ICTAC kinetics project-data, methods and results. *Thermochim Acta.* 2000;355:125–43.
32. Farjas J, Butchosa N, Roura P. A simple kinetic method for the determination of the reaction model from non-isothermal experiments. *J Therm Anal Calorim.* doi:[10.1007/s10973-010-0737-5](https://doi.org/10.1007/s10973-010-0737-5).